Zeitschrift: Helvetica Physica Acta
Band: 55 (1982)
Heft: 6

Artikel: Anisotropy of electron impurity scattering in dilute Al(Li)
Autor: Joss, W. / Mark, W. van der / Monnier, R.
DOI: https://doi.org/10.5169/seals-115310

Helvetica Physica Acta, Vol. 55 (1982) 736–754

0018–0238/82/060736–19$1.50 + 0.20/0

Anisotropy of electron impurity scattering in dilute Al(Li)

By W. Joss,[1,*,†]) W. van der Mark[2,*]) and R. Monnier,*) Laboratorium fur Festkörperphysik, Eidgenössische Technische Hochschule, CH-8093 Zürich, Switzerland
L. Cole[3,‡]) and W. E. Lawrence,‡) Department of Physics, Dartmouth College, Hanover, New Hampshire 03755, USA
and J. Deutz, Institut für Festkörperforschung der Kernforschungsanlage Jülich, D-5170, Germany

(6. I. 1983)

Abstract. The variation of the conduction electron scattering rate over the third-zone electron sheet of the Fermi surface of aluminum, due to small concentrations of lithium impurities, has been determined from de Haas–van Alphen effect studies. Theoretical results for the Dingle temperatures for orbits on the second-zone hole and third-zone electron sheet of the Fermi surface are reported. Several improvements to the previous theoretical treatment are discussed; these include nonlocal exchange and correlation in the impurity-induced potential, the effects of lattice relaxation around the impurity, and lattice backscattering. For the last point, we exploit the connection between the pseudo-plane-wave and KKR-Green's function formalisms. Despite these various improvements, the agreement between experiment and theory is not improved substantially. Possible physical reasons for this are discussed.

1. Introduction

The system Al(Li) has proven to be an interesting and stubborn testing ground for a self-consistent treatment of electron-impurity scattering, particularly as it appears in the anisotropic scattering rates of Bloch electrons on the Fermi surface in dilute alloys. The de Haas–van Alphen (dHvA) effect has become an important source of detailed information about these anisotropies [1, 2] and measures orbital averages of the scattering rates around extremal orbits on the Fermi surface in the form of Dingle temperatures

$$X_D = \frac{\hbar}{2\pi k_B} \frac{\langle \tau^{-1}(\vec{k}) \rangle}{\langle 1 + \lambda(\vec{k}) \rangle}, \tag{1}$$

*) Work supported in part by the Schweizerischer Nationalfonds zur Förderung der wissenschaftlichen Forschung.
†) Work supported in part by the U.S. Department of Energy.
‡) Work supported in part by the U.S. Department of Energy under Grant No. EY-76-S-02-2315.
1) Present address: Materials Science and Technology Division, Argonne National Laboratory, Argonne, Illinois 60439.
2) Present address: Swissair AG, CH-8152 Zürich Airport, Switzerland.
3) Present address: Solar Energy Research Institute, 1617 Cole Blvd., Golden, Colorado 80401.

where $\tau^{-1}(\vec{k})$ is the bare electron-impurity scattering rate, $1+\lambda(\vec{k})$ accounts for electron-phonon renormalization, and brackets denote the orbital average

$$\langle f(\vec{k})\rangle = \oint dk f(\vec{k}) v_\perp^{-1}(\vec{k}) / \oint dk v_\perp^{-1}(\vec{k}), \tag{2}$$

with $v_\perp(\vec{k})$ the component of electron velocity perpendicular to the applied magnetic field. These averages X_D can in principle vary considerably from orbit to orbit, and their anisotropy provides a stringent test of the theory, as our case rather well exemplifies.

As pointed out in our earlier discussion [3], the choice of Al(Li) seems ideal because the host band structure is well known, lattice relaxation around the (substitutional) impurity is negligible (as we shall discuss); and as a result we can focus our attention upon the Li impurity with its strong perturbation on the conduction electrons. Accordingly, our initial theoretical treatment [3] employed the multiple-plane-wave (MPW) formalism of Sorbello [4] to account for the aluminum band structure, but then treated the Li-induced scattering of the individual plane-wave components self-consistently, through the use of the density functional formalism of Hohenberg, Kohn and Sham [5], and using the local density approximation (LDA) for exchange and correlation. That calculation predicted a large (more than a factor of two) anisotropy for the Dingle temperatures on the third zone of the Fermi surface. In contrast almost no anisotropy is found in the experimental data.

The paper is arranged as follows. In Section 2 we discuss the preparation and characterization of the single crystals, describe the equipment and technique for evaluating the Dingle temperatures, and present the experimental results for three extremal cross sections of the third-zone Fermi surface. In Section 3 we consider several improvements to our original theoretical treatment, the most important one being the inclusion of lattice backscattering, with the result that the calculated anisotropies in X_D are only insignificantly reduced. We also critically analyse the 'on Fermi sphere' approximation inherent to the MPW formalism, and find that its effect is negligibly small. Finally, in Section 4, we draw some conclusions on the physical origin of the discrepancy between theory and experiment.

2. Experimental

2.1. *Sample preparation*

Al(Li) forms a solid solution at the low concentrations used in this study. The high vapour pressure of Li at the melting temperature of Al and the high chemical reactivity of Li make it difficult to prepare alloys without losing the solute. The losses were minimized by using graphite coated aluminum oxide molds and handling the melt in a high-purity helium atmosphere. The gas was drawn from the liquid of a helium storage dewar and was constantly exchanged. A master alloy of nominal 4 at.% Li was prepared from 99.999% pure Al[4]) in the beginning and subsequently diluted.

---

[4]) High-purity aluminum was provided by Alusuisse, Neuhausen, Switzerland

The single crystal specimens were grown by the Czochralski technique; the method of pulling crystals directly from the melt has been found to give very low dislocation densities [6, 7]. In order to avoid the tenacious oxide layer on the melt, a pair of crucibles was used. The inner crucible was filled through a hole in its bottom with shiny material, from which the crystal was grown with a diameter kept equal to the specimen size desired (1 mm for the field modulation and 5 mm for the torque method). The crystals were grown in the [100]-crystallographic direction several centimeters long and then cut to the correct length of about 5 mm by spark-erosion.

In order to get strain-free single crystals damaged regions on the surface were removed by etching. Thereafter the specimens were encapsulated in an atmosphere of argon in quartz ampoules, annealed for 64 h at a temperature of 650°C (10°C below the melting point) and slowly cooled to ambient temperature at a rate of 10°C/h. Before mounting the specimens, the crystal orientation was determined by back-reflection Laue photographs. After the dHvA experiment the actual solute concentrations were judged from measurements of the residual resistivity ratio (RRR) by an eddy current method [8] using the value 0.80 $\mu\Omega$ cm/at.% for the residual resistivity of Li in Al [9]. Table 1 shows the impurity concentration measured in this way for all samples used in the dHvA experiments.

Table 1
Li impurity concentration of Al samples, determined by residual resistivity ratio (RRR) measurements. $RRR = \rho_{300K}/\rho_{4K}$.

Sample	RRR	$\rho_{imp}[\mu\Omega\,cm]$	c[at.%][a)]
1	128	0.0209	0.0261
2	166	0.0161	0.0201
3	160	0.0167	0.0209
4	357	0.0075	0.0093

a) Using $\rho_{imp} = 0.80\ \mu\Omega$ cm/at.% from Ref. 9.

2.2. *Modulation measurements*

The sample magnetization was measured by the standard large-amplitude low-frequency field-modulation technique [10] in an iron-core electromagnet (Bruker, Karlsruhe, FRG) capable of generating 2.7 T in a 40 mm air gap with a homogeneity of better than 1×10^{-5} over a volume of 1 cm^3. The magnet current was regulated by a Hall probe stabilizing circuit and the field was kept stable to 1 part in 10^5. An NMR calibration of the field controller allowed the field to be set with an accuracy of 0.3 mT. The field was swept so that H^{-1} was linear in time. In this way the dHvA oscillations have constant frequency in time allowing prefiltering of the signal. During the sweep the magnetic field values were determined by integrating the flux from a pick-up coil.

The modulation field was generated by a pair of Helmholtz coils mounted around the pole pieces. The modulation amplitude was varied proportional to H^2 to maintain a constant Bessel-function argument. Modulation frequencies were sufficiently low (20–60 Hz) that the effects of finite penetration depth were

negligible. Signals were detected in a counterwound pair of coaxial pickup coils around the sample. Phase sensitive second harmonic detection and Bessel-function discrimination were used. The sample temperature was maintained within ±2 mK with a gas flow cryostat in the range 1.7–4.2 K. The temperature was measured with an Allen Bradley carbon resistor. The resistor was calibrated in liquid helium against the vapor pressure temperature scale. More detailed information about the dHvA spectrometer may be found in the description of Wejgaard [11].

2.3. *Torque measurements*

The torque experiments were carried out in a 10.5 T superconducting solenoid with a homogeneity of 1×10^{-6} over a volume of 1 cm^3. The homogeneity was adjusted by two compensating coils and checked over the whole field range by moving a pickup coil with constant velocity along the solenoid axis. The field was swept as H^{-1} with respect to time. The dHvA torque was measured using a capacitance technique, with a probe similar to the one described by Griessen et al. [12]. The sample holder can be rotated about an axis perpendicular to the magnetic field. The suspension system of the rotatable part of the torquemeter consisted of two identical crossed spring pairs which guarantees frictionless rotation. A pair of capacitor plates was glued between the rotatable part and the housing of the torquemeter. The torque detected as the change of capacitance was electronically compensated by a feedback system which sent a compensating current through one of two coils mounted on the torquemeter, thereby cancelling the dHvA torque with the torque resulting from the action of the magnetic field on the magnetic moment of this coil. This feedback system yields a sensitivity of 10^{-9} Nm with a torque compliance of only 10^{-2} rad/Nm.

The torquemeter was mounted in an evacuable vessel filled with helium exchange gas for thermal contact. The temperature in the liquid-helium dewar was varied between 4.2 and 1.4 K by pumping and was controlled to ±2 mK using a vacuum regulator valve. Below the λ-point of helium a capacitance thermometer served as a feedback element to a heater for fine regulation of the temperature. The sample temperature was determined by the vapor pressure of liquid helium using a Baratron capacitance manometer. A small cell containing about 0.5 cm^3 liquid helium was attached to the torquemeter which allowed an accurate determination of the vapour pressure.

2.4. *Dingle temperature evaluation*

The dHvA effect is the oscillatory variation of the magnetization of a metal with the magnetic field H. The usual formalism [13] for the interpretation of the dHvA signal is based on a formula similar to the one originally derived by Lifshitz and Kosevich [14]. The component of the oscillatory magnetization parallel to the field arising from one extremal cross section may be expressed as

$$M=\sum_{r=1}^{\infty} M_r \sin(2\pi rF/H+\beta_r), \tag{3}$$

where β_r is constant for a given orbit. The magnetization varies periodically in

H^{-1} with the dHvA frequency $F = \hbar A/2\pi e$, where A is the extremal cross-sectional area of the Fermi surface normal to H. The amplitude factor M_r depends on the ratio μ of the effective mass to the free electron value, the Dingle temperature X_D (both quantities are renormalized by the electron-phonon interaction) and on field H and temperature T in the following way:

$$M_r = D_r T(rH)^{-1/2} \exp(-r\zeta\mu X_D/H)/\sinh(r\zeta\mu T/H) \tag{4}$$

where the precise form of D_r may be found in the review by Gold [13] and $\zeta = 14.69$ T/K is a constant. Consequently, μ and X_D can be determined from the temperature and field dependences of M_r.

In dilute alloys the amplitude of the first harmonic ($r = 1$) is generally dominant and for metals with a single or with separable oscillations as the alkaline earths or noble metals the following method usually yields accurate values for μ and X_D. The effective mass ratio μ is obtained approximately from the slope of the graph of $\ln(M_1/T)$ against T at constant H, and then more precisely by choosing μ to make $\ln[M_1 \sinh(\zeta\mu T/H)/T]$ independent of T. Knowing μ, the Dingle temperature is ordinarily determined from the 'Dingle plot', the graph of $\ln[M_1 H^{1/2} \sinh(\zeta\mu T/H)]$ against H^{-1} at constant T.

In aluminium, however, a simple Dingle plot method is precluded by the number of similar frequencies with large amplitudes which are not separable, even by using the Bessel-function discrimination of the field-modulation technique. In Fig. 1 we show the five different types of orbits ($\alpha, \beta, \gamma, \xi, \psi$) observed in aluminum together with the by now classical picture of the second-zone hole sheet and the third-zone electron monster of the Fermi surface. The multiplicity of the frequency branches simultaneously arising from the α, β and γ orbits [15] of the third-zone monster is displayed in Fig. 2. The approximate position of the centres of the orbits is taken from Ref. 16. Closely lying frequencies and degenerate branches which will separate when the magnetic field does not lie in the symmetry plane are unsuitable for an accurate determination of the Dingle temperature because of the beating of the oscillations. A rough separation between the α, β and γ oscillations is possible by a suitable choice of the magnetic field range. The γ oscillations dominate the α and β oscillations at higher fields (above 1.5 T) on account of their large amplitudes and higher effective masses, whereas the α and β are best observed at fields below 1 T. Further the large-amplitude field modulation can be used to suppress one of the remaining γ oscillations. In spite of these discriminations we get a dHvA signal which simultaneously contains at least three if not five oscillations.

In order to evaluate the Dingle temperatures from such a complicated spectrum we have to fit the data record to a sum of dHvA signals. Using the definition of the sinh we rewrite equations (3) and (4) in the form (neglecting higher dHvA harmonics)

$$M = 2TH^{-1/2} \sum_i D_i \exp(-\eta_i/H)[1-\exp(-2\zeta\mu_i T/H)]^{-1} \sin(2\pi F_i/H + \beta_i), \tag{5}$$

where we sum over the observed extremal orbits and $\eta_i = \zeta\mu_i(T + X_{D_i})$ are the decay constants and D_i the experimental amplitude factors of the individual oscillations. We remain with the problem of evaluating F_i, β_i, D_i and η_i for each oscillation. The term in brackets can be adequately approximated, since the exponential is $\ll 1$ under our experimental conditions. Therefore, the effective

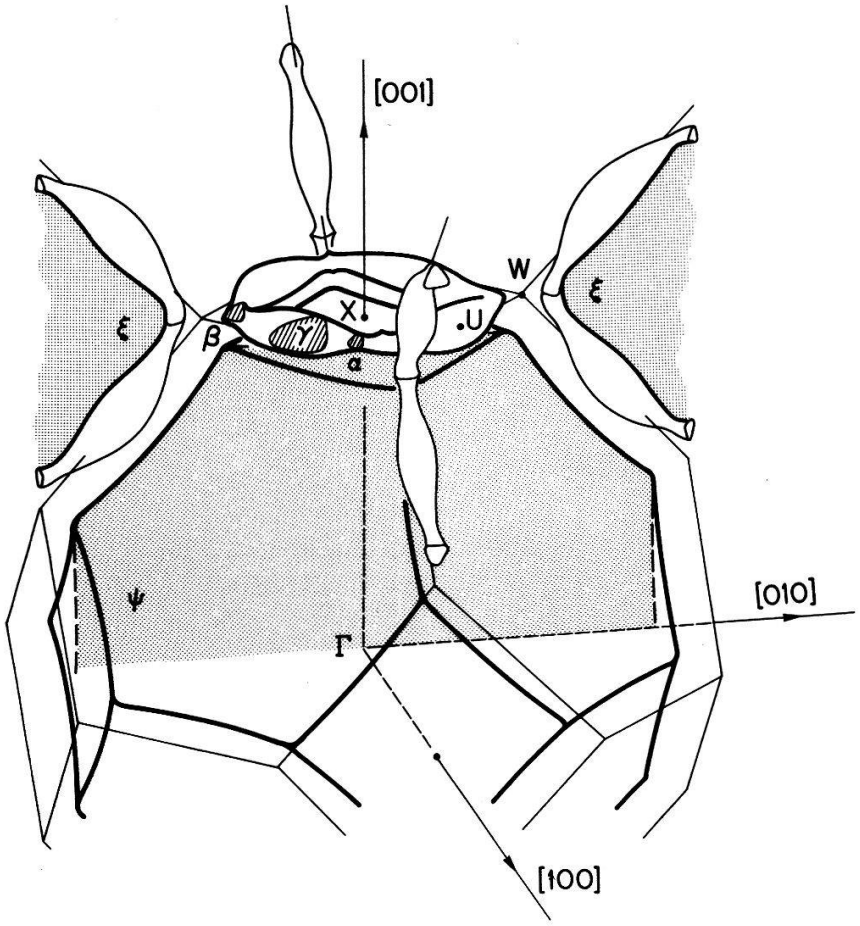

Figure 1.
Second-zone hole sheet and third-zone electron monster of the Fermi surface of aluminum. All orbits are drawn for the magnetic field in the [100] direction, except for α which merges with β for that orientation of the magnetic field and has therefore been drawn for the [110] orientation of the latter.

mass μ_i needs not be known to a great precision and can be taken from Larson and Gordon's [15] values for μ_i/F_i. They noted that the effective masses of the α, β and γ orbit vary proportional to the extremal cross-sectional area over a large range of the magnetic field orientation and that the quotient μ_i/F_i consequently is approximately constant.

The dHvA signal was measured using a minicomputer-based data-acquisition system. The data record was digitized into n data points (256 or 512 points) taken at equidistant values of H^{-1}. The sampling interval Δ was carefully chosen so that either aliasing (folding back of frequency components $>1/(2\Delta)$) in the Fourier spectrum of the data record did not occur or the aliased peaks did not overlap with other peaks. The latter case has the advantage that the low frequencies (e.g., α and β oscillations) move higher up in the spectrum. The relative resolution of the peaks is improved, and closely lying frequencies are easier to separate.

Fourier transforming the data record into frequency space gives us approximate values for the parameters F_i, β_i, D_i and η_i of the dHvA oscillations. An accurate determination of the parameters from the Fourier spectrum is impracticable since the data record has a finite length which modifies the line shape. Due to the window the Fourier transform of an exponentially damped harmonic oscillations is not a pure Lorentzian line whose half width is determined solely by the decay constant and the peaks have side lobes which may overlap partially.

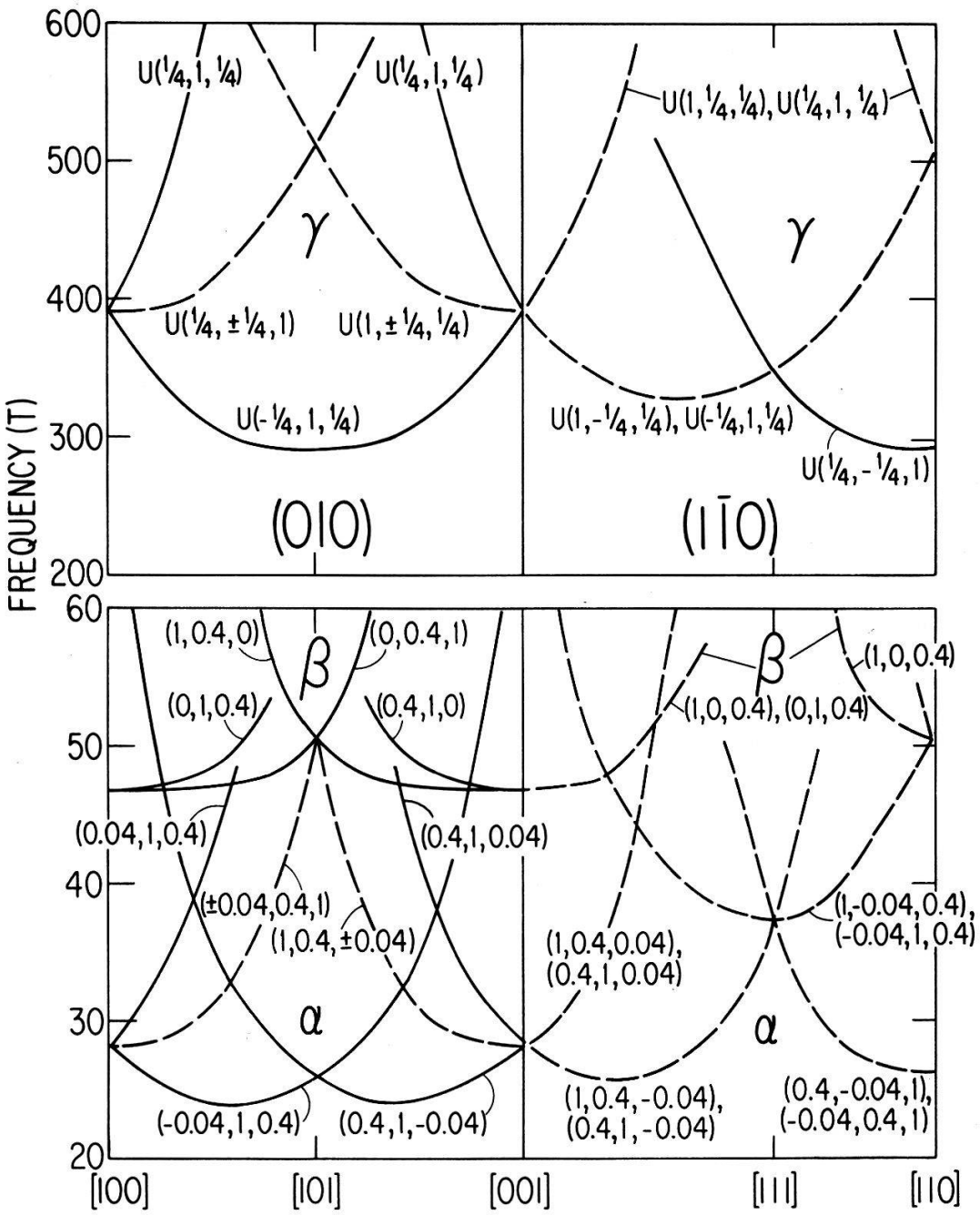

Figure 2.
dHvA frequencies associated with the third-zone of the Fermi surface of aluminum (Ref. 15) as a function of field orientation, for magnetic fields in the (010) and (110) planes. The labels on the curves refer to the approximate position of the centers of the relevant orbits in the Brillouin zone as given in Ref. 16. Branches which will separate when the magnetic field does not lie in the (010) or (110) symmetry plane are dashed.

To recover small dHvA frequency components which were buried in the side lobes of much larger components, our data were filtered using an equal-ripple finite-impulse-response digital filter [17]. The first points of the filtered output corresponding to the length of the impulse response were discarded (typically 41 of the 256 or 81 of the 512 data points). The cutoff frequency was chosen as far as possible from the dHvA frequencies of interest.

The approximate values for F_i, β_i, D_i and η_i gained from the frequency spectrum serve as good starting values for the non-linear least-squares fit of the

data record to the theoretical expression (5) of a sum of dHvA oscillations. Having measured the oscillations at different temperatures and applied our fitting procedure we finally derive the Dingle temperature X_{D_i} and the effective mass ratio μ_i for each orbit by a linear regression to

$$\eta_i(T) = \zeta\mu_i(T + X_{D_i}) \tag{6}$$

2.5. *Experimental results*

Dingle temperatures were measured in four different samples with solute concentrations up to 260 at.ppm lithium. Samples 1 and 2 listed in Table 1 were investigated with the field modulation technique and samples 3 and 4 were studied by carrying out torque experiments. Measurements were done as a function of field orientation, for magnetic fields in the (010) crystallographic plane. The α-orbit centered at $(-0.04, 1, 0.4)$ was studied with fields pointing 10° to 35° from the [100] direction, the β-orbit centered at $(0, 1, 0.4)$ with fields pointing 15° to 30° from [100], and the γ-orbit centered at $U(-1/4, 1, 1/4)$ with fields pointing 10° to 45° from [100]. Within experimental accuracy, no angular dependence of the Dingle temperatures of the α, β and γ-orbits was found. Thus crystalline mosaic structure in our specimens is unimportant, a result which was already reported for pure aluminum samples [18]. Mosaic structure would lead to a subgrain phase-smearing and introduce spurious anisotropies of the Dingle temperatures [19].

Figure 3 shows the data for three typical α, β and γ-orbits. The Dingle temperatures per at.% Li were then determined from a straight line fit to the measured Dingle temperatures as a function of the lithium concentration. The

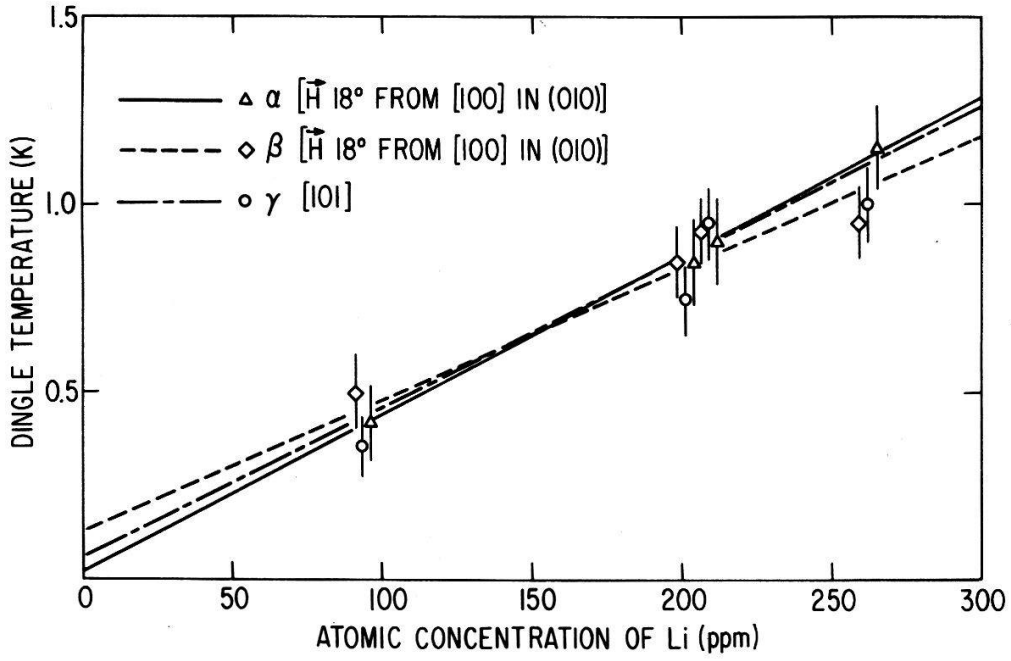

Figure 3.
Dingle temperatures (renormalized by electron-phonon interaction) for three third-zone orbits (α centered at $(-0.04, 1, 0.4)$, β at $(0, 1, 0.4)$ and γ at $U(-1/4, 1, 1/4)$) as a function of the Li concentration in aluminum. The intercept at zero concentration is due to dislocations and unknown impurities.

non-zero Dingle temperatures at zero lithium concentration are due to dislocations and unknown impurities and compare well with the values previously found in pure samples grown under the same conditions [18]. The scatter of the data points can be explained by variations of the amount of background scattering caused by dislocations, if we assume our carefully grown specimens have a constant small unknown impurity content. According to Wejgaard [11], the Dingle temperatures in dilute aluminum alloys appear to be very sensitive to dislocations.

The Dingle temperatures per at.% lithium, renormalized by the electron-phonon interaction, are listed in Table 2. The dominant source of the error in the final results is believed to arise from random variations of the dislocation density from sample to sample.

Table 2
Calculated and measured Dingle temperatures X_D for several extremal orbits in Al(Li). Present calculation accounts for lattice backscattering while that of Ref. 3 does not. Electron-phonon renormalization factors $\langle 1+\lambda(\vec{k})\rangle$ are taken from Ref. 20.

Orbit $[\vec{H}]$	Center[a] $(2\pi/a)$	$\langle 1+\lambda(\vec{k})\rangle$	X_D(K/at.% Li) Calc. Ref. 3	Calc. Present	Expt.
α[100]	(0.034, −0.41, 1)	1.48	54	55	42±5[b]
β[100]	(0, −0.42, 1)	1.48	33	38	35±8[c]
γ[110]	U(1/4, −1/4, 1)	1.38	81	76	40±5
ξ[100]	X(1, 0, 0)	1.44	58	64	
ψ[110]	Γ	1.42	45	52	
ψ[111]	Γ	1.42	40	50	

a) Ref. 16.
b) $\vec{H}$ 18° from [100] in (001)
c) $\vec{H}$ 18° from [100] in (001)

3. Theoretical

The largest discrepancy between the measured Dingle temperatures and the ones computed by Cole et al. [3] is observed for the γ [110] orbit. The apparent over-estimate of X_D for this orbit suggests that the s-wave phase shift (Table 3b) is too big: In general, the Dingle temperatures may be decomposed into sums like

$$X_D = \sum_l x_l \sin^2 \delta_l, \tag{7}$$

where δ_l are the phase shifts for scattering from the impurity-induced perturbation, and x_l are (orbit dependent) coefficients depending *only* upon the host metal (the l index refers here to orbital angular momentum, although it will be generalized later to allow for lattice backscattering). The orbital coefficients x_l are listed in Table 4c, and it is clear that the γ[110] orbit weights the s-wave phase shift heavily. Since this weighting is a property of the aluminum band structure, the problem apparently lies with the calculation of the phase shifts. Our theoretical considerations are thus focussed somewhat on the latter aspect of the problem.

3.1. *Corrections to the perturbing potential*

Besides lattice backscattering, we have considered in our improved treatment the effect of lattice relaxation around the impurity and the inclusion of exchange and correlation effects beyond the LDA, both of which involve changes in the Li-induced perturbing potential, and may be treated within the conventional multiple-plane-wave (MPW) formalism by recalculating the phase shifts. We discuss them briefly first.

The effects of non-local exchange and correlation have been examined by Cole [22], using the 'average density' approximation suggested by Gunnarsson, Jonson, and Lundqvist [23]. It was found that all the Dingle temperatures are reduced by a small amount, but the reduction is uniform and the *anisotropy* is unchanged.

Lattice relaxation of the host atoms around the Li impurity has been studied experimentally and theoretically by Solt and Werner [24]. The displacements of the neighboring shells of Al atoms are all small. The radial displacements in the (110), (200), and (220) shells are, respectively, -0.0048 Å, -0.0057 Å, and -0.0003 Å, compared with the lattice constant of about 4 Å. The other displacements are considerably smaller than these, and are negligible for our purposes. We define the applied perturbation to be the spherical average of the change in Coulomb potential arising from the displacement of these ($Z=3$) ions. This applied perturbation is essentially a set of nested square wells, with maximum depth $V_0 \approx 0.0011$ (atomic units) occurring inside the radius of the nearest neighbors. A potential with this strength, even if it were extended out to the (220) shell of neighbors, would change the phase shifts by less than 0.01 (for example, we find that $d\delta_0/dV_0 = 1.3\ \text{au}^{-1}$). This implies that the Dingle temperatures are essentially unaffected by the small amount of lattice relaxation, as we suggested earlier [3].

3.2. *Lattice backscattering*

Our self consistent treatment of the phase shifts [3] accounts for repeated scattering from the same impurity site, but assumes that the intermediate states are single plane waves (the initial and final states being Bloch waves). 'Lattice backscattering' refers to the fact that the intermediate states *should* be Bloch waves. It has been argued [3, 4, 25] that this is inconsequential for free-electron-like host metals because the intermediate states exist in all directions of $\vec{k}$-space, and most of these are free-electron-like. However, this assertion has not, to our knowledge, been tested. Sorbello's calculation [4] dealt with weak-scattering impurities for which the Born approximation was used, and so there were no intermediate states that might have 'backscattered'.

There are two methods currently in use for calculating electron-impurity scattering rates – the MPW method (used in [3, 4]) and the KKR Green's function [21, 25–27] introduced by Morgan [25]. Only the latter method properly accounts for lattice backscattering. A recent self-consistent KKR calculation for Al(Li) by Deutz [21] has provided the so-called Friedel phase shifts [1], which incorporate this effect. To show how these may be used in combination with our Fermi surface coefficients, we begin in the next paragraphs by considering the relationship between the simple metal pseudowavefunctions and the KKR wavefunctions. We

then construct the scattering rate, and eventually arrive at an expression like equation (7) involving the Friedel phase shifts together with appropriately modified Fermi surface coefficients x_L.

The pseudowavefunction for Bloch state $|\vec{k}\rangle$ in our multiple-plane-wave treatment of pure Al (normalized over the crystal volume Ω) is

$$\psi_k^{ps}(\vec{r}) = \Omega^{-1/2} \sum_{n=0}^{3} a_n(\vec{k}) e^{i(\vec{k}-\vec{g}_n)\cdot\vec{r}}, \tag{8}$$

where the sum extends over the four reciprocal lattice vectors $\vec{g}_n$ closest to $\vec{k}$. A partial wave expansion of the plane waves gives

$$\psi_k^{ps}(\vec{r}) = \frac{4\pi}{\sqrt{\Omega}} \sum_{l,m} i^l \sum_n a_n(\vec{k}) j_l(|\vec{k}-\vec{g}_n|\, r)\, Y_{lm}^*(\vec{k}-\vec{g}_n)\, Y_{lm}(\hat{r}). \tag{9}$$

This is to be compared with the KKR wavefunctions for the pure host: Inside the muffin tin radius ($r \leqslant r_{MT}$)

$$\psi_k(\vec{r}) = \sum_{l,m} i^l \alpha_{lm}(\vec{k}) R_l^h(r)\, Y_{lm}(\hat{r}), \tag{10}$$

while outside ($r \geqslant r_{MT}$) we may write [27]

$$\psi_k(\vec{r}) = \sum_{l,m} i^l \alpha_{lm}(\vec{k}) [\cos\delta_l^h j_l(\kappa r) - \sin\delta_l^h n_l(\kappa r)] Y_{lm}(\hat{r}). \tag{11}$$

The δ_l^h are the phase shifts of the host, $R_l^h(r)$ is the radial part of he wavefunction inside the host muffin tin, and j_l and n_l are spherical Bessel and Neumann functions. The wavevector κ is proportional to the square root of the energy measured with respect to the 'muffin tin zero' (the constant value of the potential between the muffin tins) and is usually different from the Fermi wavevector k_F, which measures the occupied bandwidth (here $\kappa = 0.7892$ a.u. at the Fermi level and $k_F = 0.9273$ a.u.).

Outside the atomic core radius (~1 a.u. for Al) the pseudowavefunction should be a good approximation to the true wavefunction. Thus we compare the pseudowavefunction (equation 9) with the KKR wavefunction in the interstitial region (equation 11). Their similarity is more apparent if we make the 'on Fermi sphere' approximation (soon to be relaxed) by setting $|\vec{k}-\vec{g}_n| = k_F$ in the Bessel functions of equation (9), which then becomes

$$\psi_k^{ps}(\vec{r}) = \frac{4\pi}{\sqrt{\Omega}} \sum_{l,m} i^l c_{lm}(\vec{k}) j_l(k_F r)\, Y_{lm}(\hat{r}) \tag{12}$$

where (as defined by Sorbello [4])

$$c_{lm}(\vec{k}) = \sum_n a_n(\vec{k})\, Y_{lm}^*(\vec{k}-\vec{g}_n) \tag{13}$$

Equating (11) and (12) for r evaluated at the muffin tin radius (and for states on the Fermi surface), we find

$$\alpha_{lm}(\vec{k}) = \frac{4\pi}{\sqrt{\Omega}} N_l c_{lm}(\vec{k}), \tag{14}$$

where

$$N_l = [\{\cos \delta_l^h j_l(\kappa r_{MT}) - \sin \delta_l^h n_l(\kappa r_{MT})\}/j_l(k_F r_{MT})]^{-1} \tag{15}$$

so that $\alpha_{lm} \sim c_{lm}$ for a given l. Moreover, we shall find that the electron-impurity scattering rates are independent of N_l, which eliminates the arbitrariness of the arguments $k_F r_{MT}$ and κr_{MT}.

We may now in fact relax the 'on Fermi sphere' approximation by equating equation (9) and (11) directly (again for r at the muffin tin radius, say) to get

$$\alpha_{lm}(\vec{k}) = \frac{4\pi}{\sqrt{\Omega}} N_l b_{lm}(\vec{k}), \tag{16}$$

where

$$b_{lm}(\vec{k}) = \sum_n a_n(\vec{k})\, Y_{lm}^*(\vec{k} - \vec{g}_n) j_l(|\vec{k} - \vec{g}_n|\, r_{MT})/j_l(k_F r_{MT}) \tag{17}$$

are the new effective expansion coefficients that must replace the $c_{lm}(\vec{k})$ in equation (12). We have evaluated the Dingle temperatures for a considerable range of r_{MT} values (up to the Wigner-Seitz radius R_s) using the lattice backscattering formalism to be described, and we find that they are changed by at most about 1 K/at.% Li (i.e., 2–3%) from their 'on Fermi sphere' values. Henceforth we feel justified in making the 'on Fermi sphere' approximation, and using Eq. (13). The reasons it works so well are the following: First, in the case of the p and d-waves, the Bessel functions j_1 and j_2 are slowly varying for $|\vec{k} - \vec{g}_i|$ near the Fermi momentum, and so b_{lm} and c_{lm} are approximately equal. The s-wave situation is more complicated, because $k_F R_s \approx 2.77$ is near a zero of j_0. According to our calculations, $b_{00}(\vec{k})$ differs from $c_{00}(\vec{k})$ by a factor of about 1.4 for $r_{MT} = R_s$. Remarkably, this factor is quite insensitive to the position $\vec{k}$ on the Fermi surface, and as a result, it tends to cancel out when calculating the scattering rates (for the same reason that the factor N_l of Eq. (15) cancels out). That the ratio $b_{00}(\vec{k})/c_{00}(\vec{k})$ is nearly independent of $\vec{k}$ follows from the fact that a similar ratio, namely

$$\sum_n a_n(\vec{k})\, |\vec{k} - \vec{g}_n|^2 \left(k_F^2 \sum_n a_n(\vec{k})\right)^{-1},$$

is *precisely* independent of $\vec{k}$. Its (constant) value is $1 - \sum_n V(\vec{g}_n)/\varepsilon_F = 0.8901$, where the sum is over the nonzero reciprocal lattice vectors in our 4-OPW model, and the parameters are $V(1, 1, 1) = V(1, 1, -1) = 0.009061$, $V(2, 0, 0) = 0.029147$, and $\varepsilon_F = 0.429985$ (all in atomic units). This identity is derived in the Appendix, where we also show that the ratio of $b_{00}(\vec{k})$ to $c_{00}(\vec{k})$ is 'expected' to be 1.44, which is close to the actual ratios computed from equations (13) and (17). In summary, the 'on Fermi sphere' approximation is not exact for s-waves, but it nevertheless predicts their contribution to the scattering rates to a very good approximation.

We now consider the scattering of these Bloch wavefunctions from an impurity-induced perturbation. The spherical harmonic representation of $\psi_k(\vec{r})$ is useful only in certain cases (for instance, when it is a good approximation to assume the T-matrix has full rotational symmetry). In the present case, lattice backscattering may reduce the symmetry of the T-matrix from spherical to cubic (even if the impurity-induced perturbation potential is spherically symmetric).

Such a T-matrix takes a simple form if we reexpress the Bloch wavefunctions (in equation 12, for example) in terms of cubic harmonics

$$\psi_k^{ps}(\vec{r}) = \frac{4\pi}{\sqrt{\Omega}} \sum_{l\Gamma\gamma} i^l c_{l\Gamma}^{\gamma}(\vec{k}) j_l(k_F r) Y_{l\Gamma}^{\gamma}(\hat{r}), \tag{18}$$

where Γ denotes an irreducible representation of the cubic point group, and γ is a component of Γ.

The unitary transformation from spherical to cubic harmonics is written down for example by Coleridge et al. [26] for $l \leqslant 2$. For present purposes, we need only identify the irreducible representations and list their degeneracies. The s and p waves each correspond to a single irreducible representation of either group

$$D^1 \to \Gamma_1, \qquad n(\Gamma_1) = 1 \tag{19a}$$

$$D^3 \to \Gamma_{15}, \qquad n(\Gamma_{15}) = 3 \tag{19b}$$

where $n(\Gamma)$ is the degeneracy of Γ. However, the fivefold degenerate subspace for d waves is decomposed under the lower cubic symmetry as

$$D^5 \to \Gamma_{12} \oplus \Gamma_{25'}, \qquad n(\Gamma_{12}) = 2, \quad n(\Gamma_{25'}) = 3. \tag{19c}$$

If we go to larger l, then a particular representation Γ may contain more than a single l. As long as we restrict ourselves to $l \leqslant 2$, then the MPW and KKR cubic harmonic expansion coefficients have a proportionality analogous to equation (14):

$$\alpha_{l\Gamma}^{\gamma}(\vec{k}) \sim c_{l\Gamma}^{\gamma}(\vec{k}), \quad \text{(for fixed } l\text{)} \tag{20}$$

of which we shall make use.

In terms of these KKR coefficients, the T-matrix for scattering from state $|\vec{k}\rangle$ to $|\vec{k}'\rangle$ is (following the presentation of Coleridge [1])

$$T_{kk'} = -\frac{\hbar^2}{2m\kappa} \sum_{L,\gamma} \alpha_L^{\gamma}(\vec{k}')^* \alpha_L^{\gamma}(\vec{k}) A_L \sin \Delta\delta_l e^{i\Delta\delta_l}, \tag{21}$$

where we have defined the compound index $L = (l, \Gamma)$, and the difference between the impurity and host atom phase shifts,

$$\Delta\delta_l = \delta_l^i - \delta_l^h. \tag{22}$$

The backscattering renormalization factor A_L depends only upon energy (here $\varepsilon = \varepsilon_F$) and is diagonal in L for $l \leqslant 2$ [28]. The corresponding rate of scattering from $|\vec{k}\rangle$ due to a single impurity is

$$\tau^{-1}(\vec{k}) = \frac{2\pi}{\hbar} \sum_{k'} |T_{kk'}|^2 \, \delta(\varepsilon_k - \varepsilon_{k'}) = \frac{\Omega}{4\pi^2\hbar} \int \frac{dS'}{\hbar |\vec{v}'|} |T_{kk'}|^2. \tag{23}$$

The square of $T_{kk'}$ (equation 21) generates a double summation $(L, \gamma; L', \gamma')$ but the surface integral reduces this to a single sum

$$\tau^{-1}(\vec{k}) = \frac{\Omega\hbar^3}{(4\pi m\kappa)^2} \sum_{L,\gamma} |\alpha_L^{\gamma}(\vec{k})|^2 \, |A_L|^2 \sin^2 \Delta\delta_l \int \frac{dS'}{\hbar |v'|} |\alpha_L^{\gamma}(\vec{k}')|^2. \tag{24}$$

Because the surface integral is independent of γ, we may express $\tau^{-1}(\vec{k})$ in terms

of the quantities

$$F_L(\vec{k}) = \sum_\gamma |\alpha_L^\gamma(\vec{k})|^2 \tag{25a}$$

and their Fermi surface averages

$$G_L = \int \frac{dS}{\hbar |\vec{v}|} F_L(\vec{k}) / \int \frac{dS}{\hbar |\vec{v}|} . \tag{25b}$$

For later convenience we also define the average over cyclotron orbits

$$H_L = \langle F_L(\vec{k}) \rangle, \tag{25c}$$

where brackets are defined in equation (2). Equations (25) depart slightly from Coleridge's notation, because we prefer here to work with dimensionless Fermi surface averages. Nevertheless, we continue to follow his derivation. In terms of (25a, b), the scattering rate is

$$\tau^{-1}(\vec{k}) = \frac{\pi \hbar^3 \Omega N(\varepsilon_F)}{2(m\kappa)^2} \sum_L n_L^{-1} G_L F_L(\vec{k}) |A_L|^2 \sin^2 \Delta\delta_l, \tag{26}$$

where $N(\varepsilon_F) = (2\pi)^{-3} \int dS/\hbar |\vec{v}|$ is the density of states for a single spin at the Fermi level, and n_L are the degeneracies given by equations (19a–c). On the other hand, the optical theorem requires that

$$\tau^{-1}(\vec{k}) = -\frac{2}{\hbar} \operatorname{Im} T_{kk'} = \frac{\hbar}{mk_F} \sum_L F_L(\vec{k}) \operatorname{Im} (A_L \sin \Delta\delta_l e^{i\Delta\delta_l}), \tag{27}$$

where equation (21) was used to write the second equality. Writing $A_L = |A_L| e^{i\theta_L}$ and using (26) and (27) to eliminate $|A_L|$, we find

$$\tau^{-1}(\vec{k}) = 2n_i [\pi \hbar N(\varepsilon_F)]^{-1} \sum_L n_L G_L^{-1} F_L(\vec{k}) \sin^2 (\Delta\delta_l + \theta_L), \tag{28}$$

where the Friedel phase shift

$$\phi_L = \Delta\delta_l + \theta_L \tag{29}$$

appears (their values were calculated by Deutz et al. [21], and appear on Table 3a), and where we have replaced the inverse crystal volume Ω^{-1} (representing just a single impurity in the crystal) by the actual density n_i of impurities.

Before discussing the nice properties of expression (28), we first obtain a similar one for the Dingle temperatures, by inserting equation (28) into (1) and using the definition (25c):

$$X_D = n_i [\pi^2 k_B N(\varepsilon_F) \langle 1 + \lambda(\vec{k}) \rangle]^{-1} \sum_L n_L G_L^{-1} H_L \sin^2 \phi_L. \tag{30}$$

Our present treatment hinges upon equations (28) and (30), in which the *ratios* of host-metal parameters $F_L(\vec{k})$, G_L and H_L appear. Because of this, the proportionality factors in equation (14) cancel, and so the host parameters may be calculated from either representation of the host band structure. The 4-OPW model described by Cole et al. [3] has been used to generate the Fermi surface averages G_L

Table 3(a, b)
(a) Friedel phase shifts at the Fermi level for a Li impurity in Al calculated in the KKR treatment of Ref. 21, corresponding to various representations of the cubic group, and (b) phase shifts calculated in the MPW treatment of Ref. 3. Retaining δ_3 in the MPW case affects the Dingle temperatures by much less than a percent; presumably the same would be true in the KKR case.

(a)

$L(=l\Gamma)$	$0\Gamma_1$	$1\Gamma_{15}$	$2\Gamma_{12}$	$2\Gamma_{25'}$
ϕ_L	−0.970	−0.446	−0.093	−0.166

(b)

l	0	1	2	3
δ_l	−1.214	−0.341	−0.148	−0.033

and several orbital averages H_L, and these are shown on Table 4a. Shown on Table 4b are the ratios, in the form of the host orbital parameters x_L in the KKR version of equation (7), namely

$$X_D = \sum_L x_L^{\mathrm{KKR}} \sin^2 \phi_L, \tag{31}$$

where according to equation (30),

$$x_L^{\mathrm{KKR}} = n_i[\pi^2 k_B N(\varepsilon_F)\langle 1+\lambda(\vec{k})\rangle]^{-1} n_L G_L^{-1} H_L. \tag{32}$$

By using the c_L^γ coefficients in place of the α_L^γ in equation (25a), we have made the 'on Fermi sphere' approximation. The calculation was also done without this approximation, i.e., using the b_L^γ (equation 17) for various matching radii r_{MT}. A few of the x_L^{KKR} changed by as much as 5 or 6%, but most changed by less than 3%. Within a given representation, the largest changes were generally associated with the smaller values of x_L, and so they are not reflected in the Dingle temperatures. As mentioned earlier (in the discussion following equation 17) the Dingle temperatures were all changed by at most about 1 K/at.%.

In a recent phase shift parameterization of the aluminum Fermi surface, Coleridge [29] has obtained coefficients similar to our x_L. The differences between his coefficients and ours apparently arise from the difference in Fermi surface fitting procedures and not, as questioned in [29], from the 'on Fermi sphere' approximation. The phase shift parameterization fits the Fermi surface dimensions slightly better than our 4-OPW fit, but the x_L-coefficients are not changed enough to alter our conclusions.

The x_L values in Table 4 incorporate the electron-phonon renormalization factors, which were taken from Meador and Lawrence [20]. These factors appear correctly in equations (1) and (2) provided that both the $\tau(\vec{k})$ and $v(\vec{k})$ appearing in the orbital averages are interpreted as the unrenormalized values. This is because (as explained by Poulsen et al. [30]) $v(\vec{k})$ is reduced by the factor $1+\lambda(\vec{k})$ while $\tau(\vec{k})$ is enhanced by the same factor, so that the product (which appears in the numerator of equation (1)) is unrenormalized.

Table 4(a–c)
(a) Fermi surface and orbital averages G_L and H_L (equations 25a–c) for the aluminum host, (b) orbital coefficients $x_{l\Gamma}$ (K/at.%) as defined in Eq. 32 and used with the KKR phase shifts in the present work, and (c) orbital coefficients x_l (K/at.%) as defined in equation 33 and used in the MPW calculation of Ref. 3.

		$l\Gamma$			
	Orbit [$\vec{H}$]†)	$0\Gamma_1$	$1\Gamma_{15}$	$2\Gamma_{12}$	$2\Gamma_{25'}$
(a) $G_{l\Gamma}$		0.0705	0.217	0.188	0.293
$H_{l\Gamma}$	α[100]	0.0936	0.174	0.291	0.199
	β[100]	0.0330	0.222	0.440	0.165
	γ[110]	0.1621	0.087	0.285	0.138
	ξ[100]	0.0998	0.213	0.022	0.363
	ψ[110]	0.0601	0.232	0.151	0.335
	ψ[111]	0.0438	0.272	0.028	0.429
(b) $x_{l\Gamma}^{KKR}$	α[100]	51.1	92.6	119	78.6
	β[100]	18.0	118	180	65.1
	γ[110]	94.8	49.7	125	58.4
	ξ[100]	56.0	117	9.3	147
	ψ[110]	34.2	129	64.4	138
	ψ[111]	24.9	151	12.1	176
(c) x_l^{MPW}	α[100]	42.7	81.4	303	
	β[100]	15.1	104	372	
	γ[110]	79.3	43.7	280	
	ξ[100]	46.8	102	249	
	ψ[110]	28.6	113	316	
	ψ[111]	20.8	133	300	

†) For the centers of the orbits see Table 2.

Finally, to make contact once again with the MPW formalism, we note [3, 4] that the scattering rates there depend upon the *product* of H and G, rather than on the ratio. For the sake of comparison, we write the MPW orbital factors that are used in equation (7):

$$x_l^{MPW} = 16 n_i N(\varepsilon_F)[k_B N^0(\varepsilon_F)^2 \langle 1 + \lambda(\vec{k})\rangle]^{-1} \sum_L n_L^{-1} G_L H_L, \tag{33}$$

where $N^0(\varepsilon_F) = (mk_F/2\pi^2\hbar^2)$ is the free electron density of states per spin at ε_F, and the sum is over irreducible representations Γ belonging to l. The values are listed on Table 4c. A striking feature of parts (b) and (c) of this table is that the relative weights given to s, p, and d-waves for the various orbits are similar in the two methods; this is particularly noteworthy for the s-wave coefficients of the α,β, and γ orbits. We may conclude immediately that a theoretical approach using *either* the MPW or KKR formalism must produce a small (modulo π) s-wave (Friedel) phase shift, in order to find isotropic Dingle temperatures on the third zone arms of the Fermi surface. Both calculations discussed here [3, 21] have produced large s-wave phase shifts, and thus predicted large anisotropy in the third-zone scattering rates, which is at variance with experiment (Table 2). The slightly reduced anisotropy predicted by the KKR calculation indeed stems from the difference in phase shifts, not from the difference in x-coefficients.

4. Conclusions

We have developed techniques which enable us to extract Dingle temperatures from complicated dHvA spectra. Using these techniques we have determined the Dingle temperatures in dilute Al(Li) for three typical extremal orbits (α, β, and γ) on the third-zone Fermi surface. We have found them to be isotropic to within about 20%, at variance with theoretical calculations based on both the multiple-plane-wave (MPW) and KKR formalisms which produce a factor of two anisotropy. The large predicted anisotropies stem in both cases from the large s-wave phase shifts, which are weighted most heavily on the γ-orbit, and least heavily on the β-orbit.

An advantage of the KKR formalism is that it incorporates lattice backscattering, and we believe that this is why the calculation based on it produces less anisotropy (if only slightly less) than the MPW calculation. It is tempting to conclude from a comparison of the theoretical results on Table 2 that lattice backscattering, while changing things in the right direction, is not a big enough effect to warrant further consideration. We think that such a conclusion is premature, however, because the two theoretical treatments differ not only in their account of lattice backscattering, but also in the models used for the impurity-induced potential. The KKR treatment [21, 27] includes lattice backscattering, but confines the (self-consistent) perturbing potential to the Li muffin-well. The MPW treatment ignores lattice backscattering, but allows for the redistribution of electron density and self-consistent potential beyond the Li Wigner–Seitz cell. A more realistic assessment of lattice backscattering effects might be made as follows: Recalculate the Dingle temperatures using the KKR phase shifts $\Delta\delta_l$ (i.e., neglecting the backscattering contributions θ_L), together with the MPW orbital coefficients (equation 33). Using the values obtained in [21], namely $\Delta\delta_0 = -1.297$, $\Delta\delta_1 = -0.596$, and $\Delta\delta_2 = -0.101$, we find Dingle temperatures that are all about 13–14 K/at.% larger than the KKR values listed on Table 2, so that backscattering appears to be quite significant after all.

The above considerations suggest that one might attempt to combine the advantages of *both* of the theoretical treatments presented here; for example, to include lattice backscattering by using the KKR formalism, but to allow for a self-consistent perturbation potential extending out to the neighboring muffin-wells.

We have discussed other refinements to the theoretical treatment that we feel can be safely ruled out. According to Solt and Werner [24] and our earlier discussion, lattice relaxation has a negligible effect. According to Cole [22], the effects of nonlocal exchange and correlation are small, and not such as to reduce the anisotropy.

Acknowledgements

We wish to express our gratitude to Professor J. L. Olsen for his support and continued interest throughout the course of this work. We thank Dr. W. Wejgaard for many ideas concerning the experimental techniques and the data evaluation. We wish to thank Dr. G. Lakshmi for determining the lithium content of some of the master alloys. For the skillful preparation of the samples we are

indebted to P. Caminada. Finally, we would like to thank Dr. P. T. Coleridge for stressing the potential hazards of the 'on Fermi sphere' approximation.

Appendix

We argue here that the ratio of $b_{00}(\vec{k})$ (equation 13) to $c_{00}(\vec{k})$ (equation 9) is only weakly dependent on $\vec{k}$, and arrive at an estimate of its value. The argument is based on the fact that the ratio

$$R = \sum_{n=1}^{4} a_n(\vec{k})\,|\vec{k}-\vec{g}_n|^2 \left(k_F^2 \sum_{n=1}^{4} a_n(\vec{k})\right)^{-1} \tag{A1}$$

is independent of the position $\vec{k}$ on the Fermi surface. To show this, we note first that since $a_n(\vec{k}) = \langle \vec{k}-\vec{g}_n \mid \psi_k \rangle$ is the inner product of the 4-OPW Bloch state $|\psi_k\rangle$ with the single-OPW state $|\vec{k}-\vec{g}_n\rangle$, it follows that the summand in the numerator is proportional to a kinetic energy matrix element, i.e. $a_n(\vec{k})\,|\vec{k}-\vec{g}_n|^2 = \langle \vec{k}-\vec{g}_n\,|(-\nabla^2)|\,\psi_k\rangle$. We can replace the kinetic energy operator by $H-V$, or simply by $\varepsilon_F - V$, since $|\psi_k\rangle$ has the Fermi energy. Since (by definition) $k_F^2 = 2m\varepsilon_F/\hbar^2$, we have

$$R = 1 - \sum_n \langle \vec{k}-\vec{g}_n|V|\,\psi_k\rangle \left(\varepsilon_F \sum_n a_n(\vec{k})\right)^{-1}. \tag{A2}$$

The matrix elements may be expanded to rewrite the numerator as

$$\sum_n \sum_m \langle \vec{k}-\vec{g}_n\,|V|\,\vec{k}-\vec{g}_m\rangle a_m(\vec{k}). \tag{A3}$$

The n-summation is independent of m, and for the four-OPW model, it is easily evaluated to give

$$R = 1-(2V(111)+V(200))/\varepsilon_F = 0.8901, \tag{A4}$$

where the values of the four-OPW parameters are given in the text following equation (17).

We may use (A4) to estimate the value of the ratio $b_{00}(\vec{k})/c_{00}(\vec{k})$. This is done by fitting the Bessel function $j_0(|\vec{k}-\vec{g}_n|\,r_{MT})$ to a polynomial of the form $a+b\,|\vec{k}-\vec{g}_n|^2$, in the neighbourhood of $k_F r_{MT}$; explicitely:

$$\frac{j_0(|\vec{k}-\vec{g}_n|\,r_{MT})}{j_0(k_F r_{MT})} \approx 1+\tfrac{1}{2} r_{MT} k_F \left(\frac{|\vec{k}-\vec{g}_n|^2}{k_F^2}-1\right) \frac{\partial \ln j_0(z)}{\partial z}\bigg|_{z=r_{MT}k_F}. \tag{A5}$$

Combining this with equation (A4), we find

$$\frac{b_{00}(\vec{k})}{c_{00}(\vec{k})} \approx 1 - \frac{(2V(111)+V(200))}{2\varepsilon_F}\,[r_{MT}k_F \cot(r_{MT}k_F) - 1]. \tag{A6}$$

For $r_{MT} = R_s$, the predicted value is 1.44. The actual computed ratio $b_{00}(\vec{k})/c_{00}(\vec{k})$ varies from about 1.3 to 1.5, and the ratio of orbital averages varies by less than this.

The important ratios involved in the Dingle temperatures are H_L/G_L (equations 25 and 30). These orbital averages are changed by at most 6% when the

b-coefficients are used in place of the c's. In the case of the s-waves, this depends upon the constancy of (A1). In the case of the p and d-waves, it depends upon the fact that the Bessel functions (appearing in equation (17) for $b_{lm}(\vec{k})$) are slowly-varying.

REFERENCES

[1] P. T. COLERIDGE in: *Electrons at the Fermi surface*, ed. M. Springford, Cambridge University Press, Cambridge, 1980, pp. 321–61.
[2] M. SPRINGFORD in: *Electrons at the Fermi surface*, ed. M. Springford, Cambridge University Press, Cambridge, 1980, pp. 362–92.
[3] LEE COLE, W. E. LAWRENCE, R. MONNIER, W. JOSS, W. VAN DER MARK and M. MANNINEN, Phys. Rev. Lett. *42* (1979) 1174–8.
[4] R. S. SORBELLO, J. Phys. F: Metal Phys. *4* (1974) 1665–83.
[5] P. HOHENBERG and W. KOHN, Phys. Rev. *136* (1964) B864–71; W. Kohn and L. J. Sham, Phys. Rev. *140* (1965) A1133–8.
[6] S. HOWE and C. ELBAUM, Phil. Mag. *6* (1961) 1227–40.
[7] R. A. PHILLIPS and A. V. GOLD, Phys. Rev. *178* (1969) 932–52.
[8] W. WEJGAARD and V. S. TOMAR, J. Phys. E: Sci. Instr. *7* (1974) 395–9.
[9] S. CERESARA, A. GIARDA and A. SANCHEZ, Phil. Mag. *35* (1977) 97–110.
[10] A. GOLDSTEIN, S. J. WILLIAMSON and S. FONER, Rev. Sci. Instr. *36* (1965) 1356–65.
[11] W. WEJGAARD, *Doctoral dissertation Eidgenössische Technische Hochschule*, Zürich (1975).
[12] R. GRIESSEN, M. J. G. LEE and D. J. STANLEY, Phys. Rev. *B16* (1977) 4385–99.
[13] A. V. GOLD in: *Solid State Physics, Vol. 1, Electron in Metals*, ed. J. F. Cochran and R. R. Haering, Gordon and Breach, New York, 1968, pp. 39–126.
[14] I. M. LIFSHITZ and A. M. KOSEVICH, Zh. Eksp. Teor. Fiz. *29* (1955) 730; Sov. Phys.—JETP (English Transl.) *2* (1956) 636–45.
[15] C. O. LARSON and W. L. GORDON, Phys. Rev. *156* (1967) 703–15.
[16] W. JOSS and R. MONNIER, J. Phys. F: Metal Phys. *10* (1980) 9–31.
[17] L. R. RABINER and B. GOLD, *Theory and Application of Digital Signal Processing*, Prentice Hall, Englewood Cliffs, New Jersey, 1975, pp. 75–204.
[18] W. VAN DER MARK and W. WEJGAARD, Helv. Phys. Acta *48* (1975) 431–4.
[19] K. M. MILLER, R. G. POULSEN and M. SPRINGFORD, J. Low Temp. Phys. *6* (1972) 411–23.
[20] A. B. MEADOR and W. E. LAWRENCE, Phys. Rev. *B15* (1977) 1850–8.
[21] J. DEUTZ, unpublished.
[22] LEE A. COLE, Ph.D. Thesis, Dartmouth College (1979), available from University Microfilms, Ann Arbor, Mich.; Bull. Am. Phys. Soc. *25* (1980) 276; and Technical Report COO-2315-14, Dartmouth College (1981).
[23] O. GUNNARSSON, M. Jonson and B. I. LUNDQVIST, Phys. Lett *59A* (1976) 177–9; and Solid State Commun. *24* (1977) 765–8.
[24] G. SOLT and K. WERNER, Phys. Rev. *B24* (1981) 817–34.
[25] G. J. MORGAN, Proc. Phys. Soc. *89* (1966) 365–71.
[26] P. T. COLERIDGE, N. A. W. HOLZWARTH and M. J. G. LEE, Phys. Rev. *B10* (1974) 1213–29.
[27] R. PODLOUCKY, R. ZELLER and P. H. DEDERICHS, Phys. Rev. *B22* (1980) 5777–90.
[28] J. W. BLAKER and R. HARRIS, J. Phys. C: Solid State Phys. *4* (1971) 569–76.
[29] P. T. COLERIDGE, J. Phys. F: Metal Phys. *12* (1982) 2563–78.
[30] R. G. POULSEN, D. L. RANDLES and M. SPRINGFORD, J. Phys. F: Metal Phys. *4* (1974) 981–98.